Article

Cell Reports

Presenilin 2 Modulates Endoplasmic Reticulum-Mitochondria Coupling by Tuning the Antagonistic Effect of Mitofusin 2

Graphical Abstract

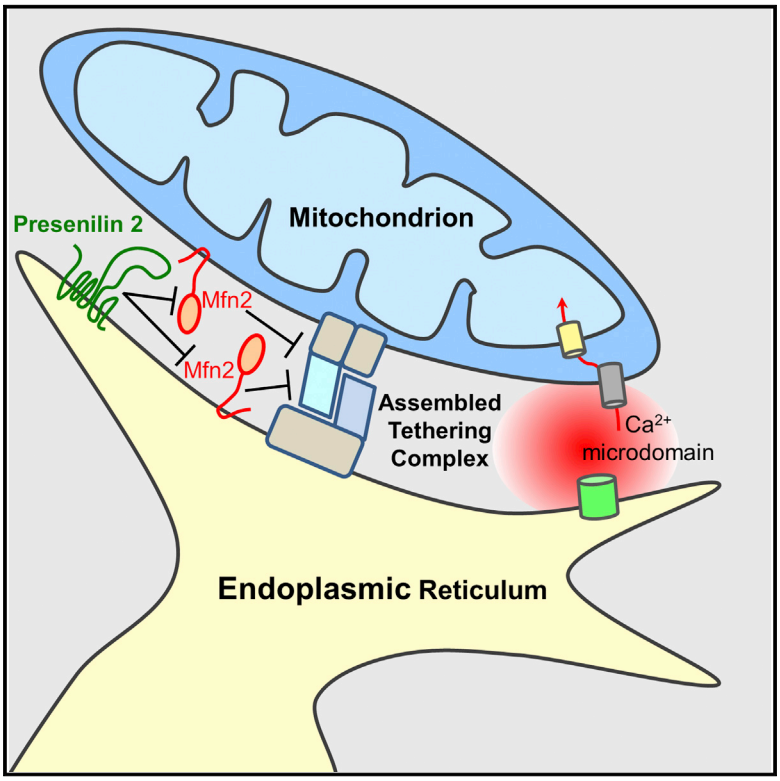

Authors

Riccardo Filadi, Elisa Greotti, Gabriele Turacchio, Alberto Luini, Tullio Pozzan, Paola Pizzo

Correspondence

paola.pizzo@unipd.it

In Brief

Filadi et al. find that the familial Alzheimer's disease (FAD)-related protein Presenilin 2, enriched at mitochondria-associated membranes, positively modulates endoplasmic reticulum (ER)-mitochondria coupling by binding to Mitofusin 2 and blocking its negative effects on organelle tethering.

Highlights

- Presenilin 2 (PS2) needs Mitofusin 2 (Mfn2) to modulate ER-mitochondria coupling
- PS2 interacts with Mfn2 and blocks its negative activity on organelle tethering
- PS1 and Mfn1 are dispensable for this molecular interplay
- Alzheimer's disease PS2 mutants bind Mfn2 more efficiently at MAMs

Filadi et al., 2016, Cell Reports *15*, 2226–2238
June 7, 2016
http://dx.doi.org/10.1016/j.celrep.2016.05.013

CellPress

OPEN ACCESS
CellPress

Cell Reports
Article

Presenilin 2 Modulates Endoplasmic Reticulum-Mitochondria Coupling by Tuning the Antagonistic Effect of Mitofusin 2

Riccardo Filadi,[1] Elisa Greotti,[1,4] Gabriele Turacchio,[2] Alberto Luini,[2] Tullio Pozzan,[1,3,4] and Paola Pizzo[1,*]
[1]Department of Biomedical Sciences, University of Padua, via U. Bassi 58/B, Padua 35131, Italy
[2]Department of Biomedical Sciences, Institute of Protein Biochemistry, Italian National Research Council (CNR), via P. Castellino 111, Naples 80131, Italy
[3]Venetian Institute of Molecular Medicine, via Orus 2, Padua 35131, Italy
[4]Department of Biomedical Sciences, Institute of Neuroscience, Italian National Research Council (CNR), via U. Bassi 58/B, Padua 35131, Italy
*Correspondence: paola.pizzo@unipd.it
http://dx.doi.org/10.1016/j.celrep.2016.05.013

SUMMARY

Communication between organelles plays key roles in cell biology. In particular, physical and functional coupling of the endoplasmic reticulum (ER) and mitochondria is crucial for regulation of various physiological and pathophysiological processes. Here, we demonstrate that Presenilin 2 (PS2), mutations in which underlie familial Alzheimer's disease (FAD), promotes ER-mitochondria coupling only in the presence of mitofusin 2 (Mfn2). PS2 is not necessary for the antagonistic effect of Mfn2 on organelle coupling, although its abundance can tune it. The two proteins physically interact, whereas their homologues Mfn1 and PS1 are dispensable for this interplay. Moreover, PS2 mutants associated with FAD are more effective than the wild-type form in modulating ER-mitochondria tethering because their binding to Mfn2 in mitochondria-associated membranes is favored. We propose a revised model for ER-mitochondria interaction to account for these findings and discuss possible implications for FAD pathogenesis.

INTRODUCTION

The communication between intracellular organelles and their functional interplay at specific membrane contact sites have acquired a marked importance in biological research. In particular, a continuous privileged relationship exists between the endoplasmic reticulum (ER) and mitochondria, which is essential for several cell functions, such as lipid metabolism (Bionda et al., 2004; Rusiñol et al., 1994; Vance, 1990), modulation of Ca^{2+} signaling (Contreras et al., 2010; Pizzo et al., 2012), mitochondrial activity (Cárdenas et al., 2010; Glancy and Balaban, 2012) and shaping (Friedman et al., 2011; Korobova et al., 2013), autophagy (Hamasaki et al., 2013; Westermann, 2010), and cell survival and death (Bravo et al., 2011; Cárdenas et al., 2010; Contreras et al., 2010; see also Hayashi et al., 2009; Marchi et al., 2014; Rowland and Voeltz, 2012; and Vance, 2014 for recent reviews).

Several proteins are believed to be involved in linking these two organelles. In yeast, the ERMES complex physically tethers ER and mitochondria membranes, and its absence results in the dysfunctional phospholipid biosynthesis (Kornmann et al., 2009). Mammalian homologs of the ERMES complex have not been identified yet, but a similar function has been attributed to mitofusin 2 (Mfn2), a mitochondrial and ER membrane protein involved in mitochondrial fusion (Hoppins et al., 2007). According to this view, Mfn2, at the level of the specific ER membrane domains called mitochondria-associated membranes (MAMs), makes homotypic interactions with mitochondrial Mfn2, as well as hetero-complexes engaging its homolog Mfn1 on mitochondria (de Brito and Scorrano, 2008). This model has been challenged, however, by a quantitative electron microscopy (EM) analysis, showing that, in *Mfn2*$^{-/-}$ cells compared to wild-type (WT), there is an increase (and not a decrease) in the number of close contacts between the two organelles (Cosson et al., 2012). Moreover, we (Filadi et al., 2015) and others (Li et al., 2015; Wang et al., 2015) have presented multiple biochemical, morphological, functional, and genetic data demonstrating that Mfn2 acts as a tethering antagonist that prevents excessive and potentially toxic proximity between the two organelles. In mammalian cells, many proteins localize at MAMs and physically interact with specific molecular partners (see Marchi et al., 2014, and Raturi and Simmen, 2013, for reviews), but it remains unclear whether these proteins are components of a single tether structure or whether they exist in separate complexes, not all directly involved in the formation of ER-mitochondria physical bridges.

The two ubiquitous proteins presenilin 1 and 2 (PS1 and PS2), whose mutations are causally linked to familial Alzheimer's disease (FAD), also are enriched in MAMs (Area-Gomez et al., 2009). PSs are essential components of the γ-secretase complex responsible for the production of β-amyloid (Aβ) peptides, which eventually accumulate into cerebral amyloid plaques characterizing the disease (Goedert and Spillantini, 2006). The γ-secretase activity has been found in MAMs, leading to a localized Aβ production that could affect ER and mitochondrial functions (Schreiner et al., 2015). Moreover, at the same intracellular

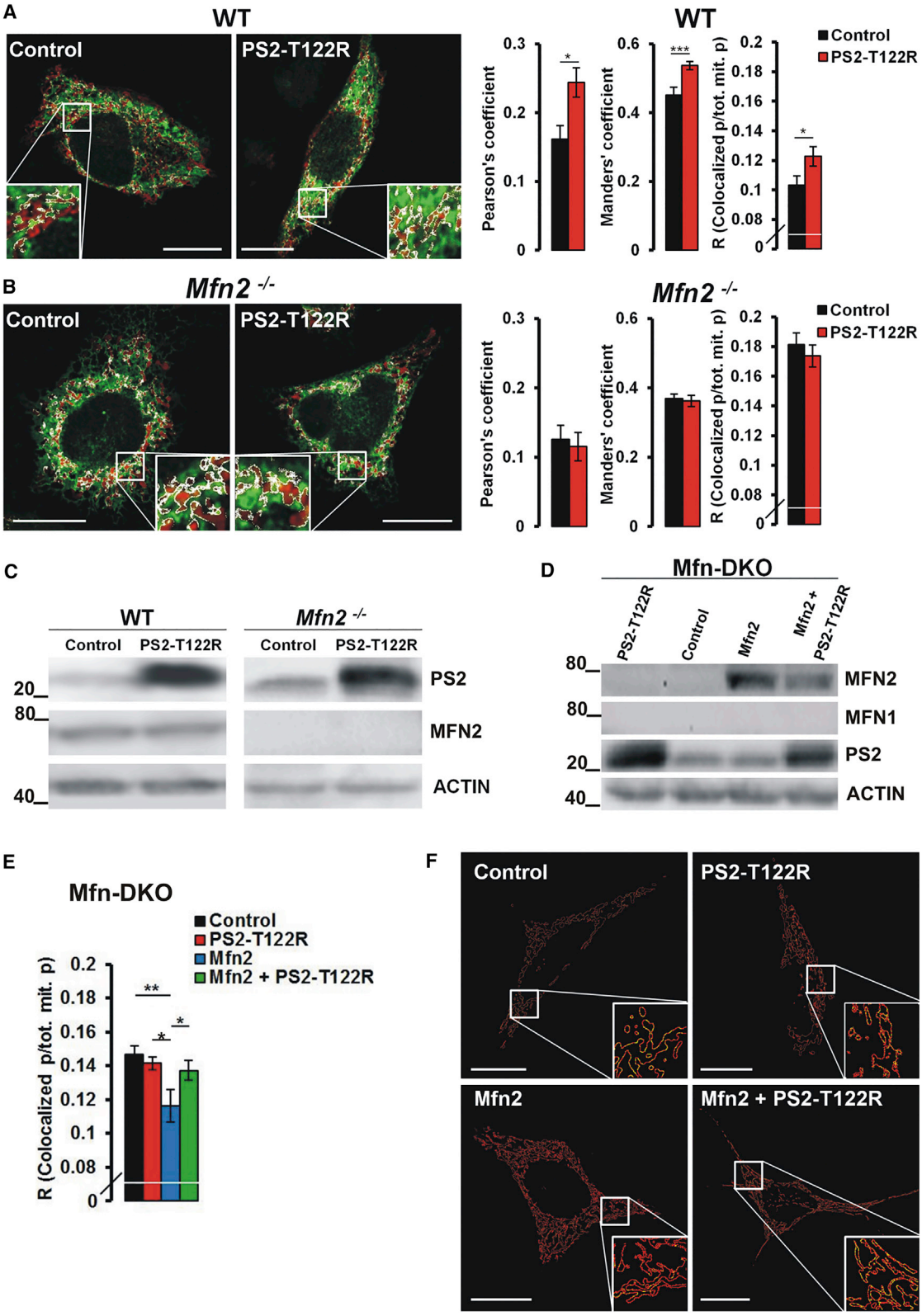

(legend on next page)

location, we have described a different role for PS2 that is independent from its γ-secretase activity: PS2, but not PS1, modulates ER-mitochondria tethering and Ca^{2+} crosstalk between these organelles, with FAD-linked PS2 mutants more potent than their WT counterpart in this function (Zampese et al., 2011).

Here we show that the PS2-favoring ER-mitochondria tethering effect depends on Mfn2: in particular, PS2 is able to increase ER-mitochondria juxtaposition, whereas its depletion decreases this coupling, only in the presence of Mfn2. In contrast, Mfn2 antagonizes ER-mitochondria tethering even in the absence of PS2, although this effect is tuned by PS2 abundance. Notably, the two proteins physically interact and their homologs Mfn1 and PS1 are not engaged in this interplay. Finally, we show that FAD-linked PS2 mutants are more enriched in MAMs than the WT form and, thus, their binding to Mfn2 is favored, resulting in a more potent modulation of ER-mitochondria tethering. These effects are present not only in PS2-overexpressing cells but also in human FAD fibroblasts that are heterozygotes for the PS2-N141I mutation. These findings lead to a revised model for ER-mitochondria tethering, revealing an essential role for PS2 in cell physiology and suggesting an additional molecular mechanism through which FAD-PS2 mutations can lead to the pathology of AD.

RESULTS

PS2 Needs Mfn2, but Not Mfn1, to Regulate ER-Mitochondria Tethering

PS2, either WT or FAD mutant, is highly expressed at ER membranes (Figure S1A), although its distribution is not homogeneous and tends to form clusters, frequently corresponding to points in which ER contacts mitochondria (white arrows, Figure S1A). Interestingly, Pearson's co-localization coefficient revealed a tendency of FAD-PS2 mutant to better co-localize with mitochondria compared to WT protein (Figure S1B). Since one of the major master regulators of ER-mitochondria tethering is Mfn2 (de Brito and Scorrano, 2008), we investigated whether the mechanism by which PS2 modulates ER-mitochondria coupling (Kipanyula et al., 2012; Zampese et al., 2011) requires the presence and/or the co-operation of Mfn2. This latter protein has been suggested to play a key role in ER-mitochondria juxtaposition, although contrasting results on its role have been reported. In particular, we and others (Cosson et al., 2012; Filadi et al., 2015; Li et al., 2015; Wang et al., 2015) have demonstrated that Mfn2 exerts a negative, and not a positive (de Brito and Scorrano, 2008), effect on the coupling between these organelles.

ER-mitochondria contacts were evaluated by confocal microscopy in mouse embryonic fibroblasts (MEFs), WT or knockout (KO) for Mfn2 ($Mfn2^{-/-}$), co-transfected with the FAD-PS2-T122R mutant (a PS2 mutant with particularly strong effects on Ca^{2+} homeostasis and ER-mitochondria tethering [Zampese et al., 2011; Zatti et al., 2006]), a mitochondria-targeted red fluorescent protein (RFP) (mt-RFP), and an ER-targeted GFP (ER-GFP; Figures 1A and 1B, left, and 1C). Multiple co-localization analyses (Manders', Pearson's correlation coefficients, and coefficient R that determines the extent of mitochondrial perimeter in contact with the ER [Filadi et al., 2015]; see also the Experimental Procedures) revealed a significant increase in ER-mitochondria co-localization upon FAD-PS2-T122R expression in WT, but not in $Mfn2^{-/-}$, MEFs (Figures 1A and 1B, right). The lack of the PS2-dependent potentiation of ER-mitochondria coupling in $Mfn2^{-/-}$ MEFs is not due to clonal adaptation, because it also was observed in MEFs deficient in both Mfn1 and Mfn2 (Mfn-double knockout [DKO] MEFs; Figures 1D and 1E). The ability of PS2 to potentiate ER-mitochondria coupling was rescued only when Mfn2 was jointly re-expressed in Mfn-DKO MEFs (Figure 1E). In these cells the extent of ER-mitochondria interaction was significantly decreased when Mfn2 was re-expressed alone (as it has been demonstrated previously [Filadi et al., 2015]), but recovered upon Mfn2 and FAD-PS2 co-expression (Figures 1E and 1F). In these latter experiments, in which Mfn2 re-expression induces marked changes in mitochondrial morphology, only the perimeter coefficient (R) was calculated (see the Experimental Procedures). Indeed, as previously reported (Filadi et al., 2015), classical Manders' and Pearson's co-localization coefficients are useful tools whenever no marked changes in ER/mitochondria morphology occur (as in the case of PS2 expression); on the contrary, in the presence of gross organelle morphology alterations (such as upon Mfn2 ablation/expression), they are prone to artifacts.

The above data were confirmed by quantitative EM analysis. PS2 overexpression increased ER-mitochondria tethering, visualized by EM as an increase in close contacts between the two organelles (distance $\leq$ 15 nm), only in WT and not in $Mfn2^{-/-}$ MEFs (Figure 2). Given the reported existence of different types of ER-mitochondria contacts (Csordás et al., 2006; Filadi et al., 2015), medial- (20–40 nm) and long- (50–100 nm) distance regions of apposition between ER and mitochondria also were analyzed. We found that, in WT MEFs, the first type of contacts are particularly rare (<7% of mitochondria display a contact with the ER in this range of distance, data not shown), while long-distance regions are more frequent and usually more extended than the close contacts (mean lengths were 250 and 100 nm, respectively), but they were not modified by PS2 overexpression (Table S1).

Because $Mfn2^{-/-}$ MEFs have more ER-mitochondria juxtapositions than WT MEFs (as we previously reported [Filadi et al.,

Figure 1. PS2 Needs Mfn2 to Exert Its ER-Mitochondria Tethering Effect

(A and B) ER-mitochondria interactions in WT (A) and $Mfn2^{-/-}$ (B) MEFs upon co-expression of mt-RFP, ER-GFP, and PS2-T122R, as revealed by confocal microscopy. Scale bar, 10 μm. Here and in the following figures, highlighted boxes show cellular zones at higher magnification to better visualize the ER-mitochondria vicinity (white pixels) in the different conditions. Co-localization indexes, Pearson's, Manders', and the perimeter coefficient R, calculated from entire single confocal images, are shown (right) for each condition. Mean ± SEM; n = 24–40 cells, imaged in three independent experiments.

(C and D) Representative (of at least five experiments) western blots of WT, $Mfn2^{-/-}$ (C), and Mfn-DKO (D) MEFs, transfected as indicated, are shown.

(E and F) ER-mitochondria interactions in Mfn-DKO MEFs were quantified (E) for the indicated conditions by the coefficient R (mean ± SEM; n = 12–21 cells) from confocal images (F) of cells co-expressing mt-RFP and ER-GFP, imaged in three independent experiments. Red pixels correspond to the whole mitochondrial perimeter profiles, and yellow pixels represent the points in which mitochondrial perimeter is in contact with the ER. Scale bar, 10 μm. Linked to Figure S1.

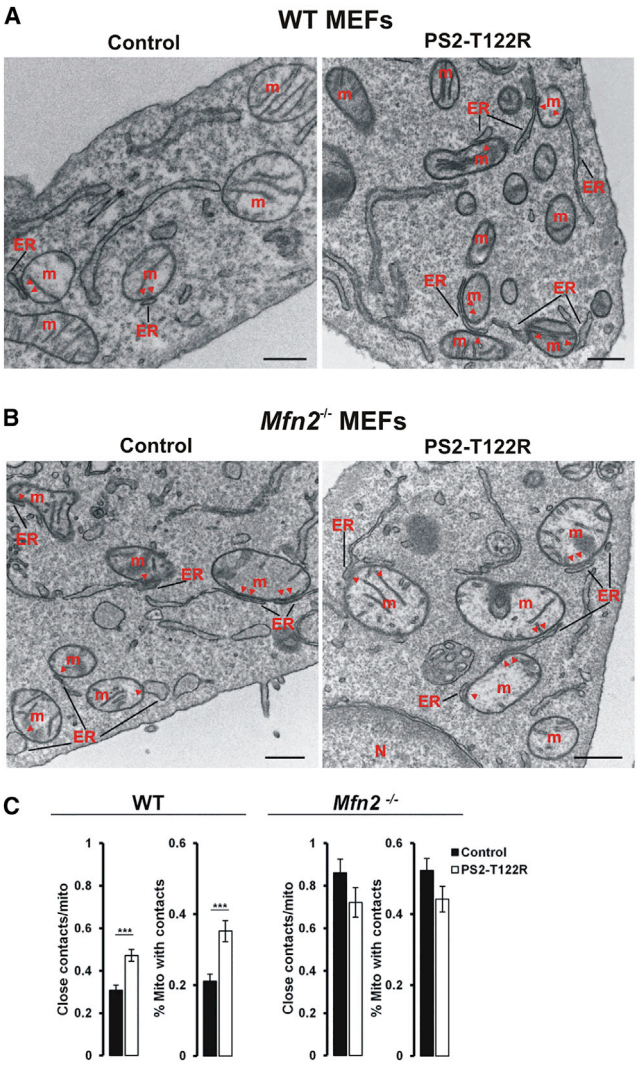

Figure 2. PS2-T122R Expression Increases ER-Mitochondria Close Contacts Only in the Presence of Mfn2

(A and B) Representative EM images of WT (A) and *Mfn2*$^{-/-}$ (B) MEFs, expressing, or not (control), PS2-T122R (n = 3 independent experiments for each condition). Scale bar, 0.5 μm. (A) Several close appositions (distance ≤15 nm, red arrowheads) are visible between ER cisternae and mitochondria (m) in control WT MEFs and, more frequently, in PS2-T122R-expressing cells. (B) In *Mfn2*$^{-/-}$ MEFs, PS2-T122R expression does not increase the number of close appositions. In these cells, ER membranes appear swollen. N, nucleus.

(C) Bars represent the average number of close contacts/mitochondrion (left) and the average percentage of mitochondria with close contacts/cell (right) observed in WT and *Mfn2*$^{-/-}$ MEFs expressing, or not, PS2-T122R (mean ± SEM; n = 20–30 cells in three independent experiments).

2015] and confirm here; see coefficient R in Figures 1A, 1B, and 2C), we reasoned that the ER-mitochondria tethering effect of PS2 could not be observed in *Mfn2*$^{-/-}$ MEFs because the extent of contacts that could be formed was somehow saturated. To address this point, endogenous PS2 was silenced by specific small interfering RNA (siRNA): whereas WT MEFs showed decreased ER-mitochondria appositions (as previously shown in other cell lines [Zampese et al., 2011]; Figure S2A), no effect was observed in *Mfn2*$^{-/-}$ MEFs (Figure S2B). Together these results demonstrate that PS2 needs Mfn2, not Mfn1, to modulate ER-mitochondria tethering.

The Antagonistic Effect of Mfn2 on ER-Mitochondria Tethering Is Modulated by PS2 Expression Levels

To investigate whether PS2 is needed for Mfn2-dependent effects on ER-mitochondrial tethering, the knockdown approach was used, because Mfn2 overexpression in WT cells induces marked mitochondria aggregation (Filadi et al., 2015) that eventually leads to mitochondrial dysfunction and cell death (Huang et al., 2007; Rojo et al., 2002; Santel and Fuller, 2001). Mfn2 silencing increased ER-mitochondria apposition in MEFs deficient in both PS1 and PS2 (PS-DKO [Brunello et al., 2009]; Figures S2D and S2E), as it did in WT cells (Filadi et al., 2015), indicating that Mfn2 can inhibit coupling between these organelles in the absence of PS2. However, quantitative EM revealed that PS2 abundance can tune the Mfn2 activity as a tethering inhibitor: Mfn2 silencing induced an increase in the number of close contacts between ER and mitochondria in WT MEFs (Filadi et al., 2015), but not in PS2-overexpressing MEFs (Figure S2C). Moreover, in *Mfn2*$^{-/-}$ MEFs, the antagonistic effect on ER-mitochondria tethering of Mfn2 re-expression (previously shown in Filadi et al., 2015) was dampened by the concomitant expression of PS2-T122R (Figure S2F), further suggesting that the two proteins may impinge on the same pathway that modulates organelles' tethering.

The ability of PS2 to modulate ER-mitochondria tethering does not rely on regulation of Mfn2 protein expression and stability. Indeed, Figure S2G shows that Mfn2 turnover is not altered by PS2 expression: upon protein synthesis inhibition, the amount of Mfn2 over time was not significantly different in control and PS2-T122R-expressing cells.

PS2 Modulates ER-Mitochondria Ca^{2+} Crosstalk Only in the Presence of Mfn2

Conditions that increase ER-mitochondria apposition also should favor Ca^{2+} transfer between the organelles, a process that largely depends on the formation of Ca^{2+} hotspots on the outer mitochondrial membrane (OMM) (Csordás et al., 2010; Giacomello et al., 2010). In WT MEFs expressing cytosolic (cyt-Aeq) or mitochondria-targeted aequorin (mit-Aeq), as Ca^{2+} probes, and PS2-T122R (Figures 3A and 3C), the amplitude of cytosolic Ca^{2+} peaks in response to stimulation with ATP, an IP_3-generating agonist, is reduced compared to controls (Figures 3A, inset, and 3C, left), as previously shown (Brunello et al., 2009; Zatti et al., 2006). However, as reported before (Zampese et al., 2011), when the amplitude of cytosolic Ca^{2+} peaks of controls is reduced by a pre-depletion protocol (see the Experimental Procedures) to match that of the FAD-PS2-expressing cells, the mitochondrial Ca^{2+} peaks of the latter cells are substantially increased (Figure 3A, red traces) compared to those of pre-depleted controls (Figures 3A, blue traces, and 3C, right).

The potentiating PS2-T122R-mediated effect on ER-mitochondria Ca^{2+} transfer was maintained even when a different experimental protocol to reduce the ER Ca^{2+} content of controls was employed (Figures S3B and S3C; see the Experimental

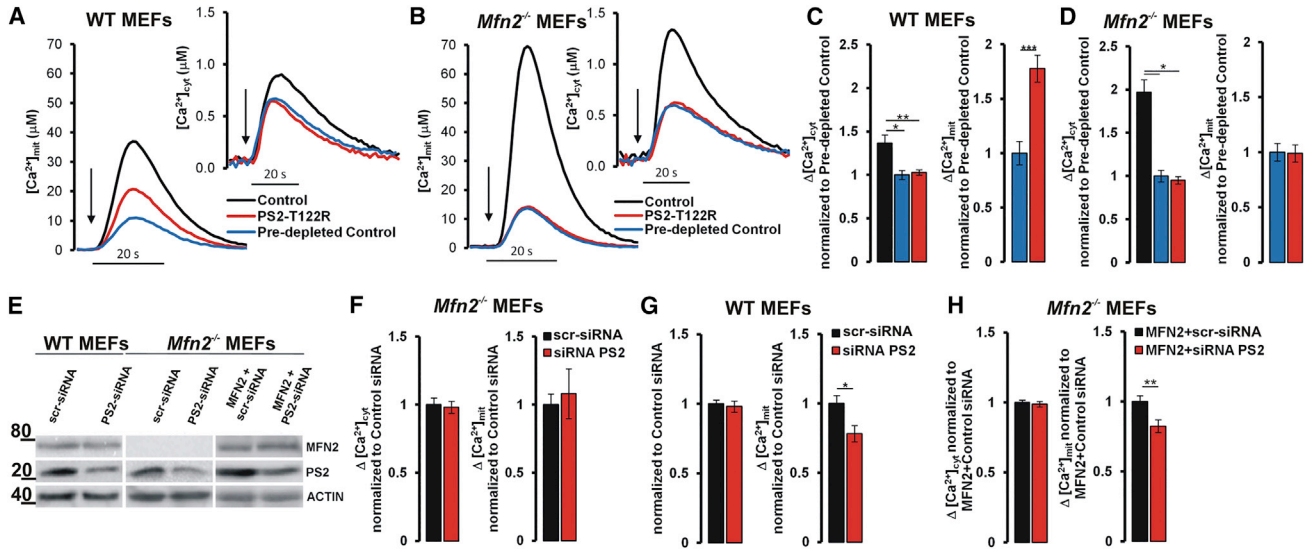

Figure 3. PS2 Modulates ER-Mitochondria Ca^{2+} Crosstalk Only in the Presence of Mfn2

Different MEFs (as indicated in each panel) were analyzed for cytosolic Ca^{2+} ($[Ca^{2+}]_{cyt}$) and mitochondrial Ca^{2+} ($[Ca^{2+}]_{mit}$) changes by cyt-Aeq and mit-Aeq, respectively. Pre-depleted control cells were pre-incubated in a Ca^{2+}-free, EGTA-containing medium for a fixed period of time so that they released similar amounts of cytosolic Ca^{2+} as PS2-overexpressing cells.

(A and B) Representative cytosolic (inset) and mitochondrial Ca^{2+} traces in control (black), pre-depleted control (blue), and PS2-T122R-overexpressing (red) WT (A) or *Mfn2*$^{-/-}$ (B) MEFs, bathed in Ca^{2+}-free, EGTA-containing medium and challenged with ATP (where indicated by the arrow), are shown.

(C and D and F–H). Bars represent mean $[Ca^{2+}]_{cyt}$ (left) and $[Ca^{2+}]_{mit}$ (right) peaks upon ATP stimulation in the different conditions (mean ± SEM; n = 3–13 independent experiments per condition).

(E) Representative (n = 3 for each condition) western blot of WT and *Mfn2*$^{-/-}$ MEFs, transfected as indicated, is shown. Linked to Figures S2 and S3.

Procedures). Importantly, a similar ER Ca^{2+} content was present in both PS2-T122R-expressing and pre-depleted control cells (verified by measuring ATP-induced cytosolic Ca^{2+} release after cell treatment with FCCP, thus blocking the possible buffering effect due to mitochondrial Ca^{2+} uptake) (Figure S3A). Moreover, neither Ca^{2+} influx through the plasma membrane (Figures S3D and S3E) nor ionomycin-induced ER Ca^{2+} release (which does not depend on the physiologically relevant ER channels; Figures S3F and S3G) elicited significantly different mitochondrial Ca^{2+} peaks between PS2-T122R-expressing and control cells. Thus, PS2-T122R expression does not affect the capacity and affinity of the mitochondrial Ca^{2+} uptake machinery (as previously demonstrated by Zampese et al., 2011) and the PS2-mediated strengthening of ER-mitochondria Ca^{2+} transfer is specifically due to an increased physical interaction between the two organelles.

In contrast, FAD-PS2 expression in *Mfn2*$^{-/-}$ MEFs reduced the ATP-induced cytosolic Ca^{2+} peaks (Figures 3B, inset, and 3D, left), as in WT MEFs, but did not potentiate the mitochondrial Ca^{2+} peaks (Figures 3B and 3D, right). Similar results were obtained expressing another FAD-PS2 mutant (N141I), which was effective in WT MEFs and other cells (Zampese et al., 2011), but not in *Mfn2*$^{-/-}$ MEFs (Figures S4A–S4C) and in MEFs deficient for both Mfn1 and Mfn2 (Mfn-DKO MEFs) expressing PS2-T122R (Figure S4D). The lack of effect of PS2-T122R on mitochondrial Ca^{2+} uptake in Mfn-DKO MEFs was reversed by Mfn2 re-expression (Figure S4E). In addition, ATP induced an increase in the mitochondrial Ca^{2+} peak in Mfn-DKO MEFs when PS2 was co-expressed with two Mfn2 mutants that were targeted to either the surface of mitochondria (Mfn2ActA) or the ER (Mfn2IYFFT) (de Brito and Scorrano, 2008) (Figure S4F), but not when PS2 was co-expressed only with mitochondria-targeted Mfn2 (Figure S4G) or ER-targeted Mfn2 (Figure S4H). Similar results were obtained with *Mfn2*$^{-/-}$ MEFs expressing PS2-T122R and, respectively, only the mitochondria-targeted Mfn2 (Figure S4I) or the ER-targeted Mfn2 (Figure S4J). These results indicate that PS2 needs Mfn2, both in *cis* and in *trans*, to exert its modulation on ER-mitochondria functional coupling and that endogenous Mfn1 is dispensable. Indeed, *Mfn1*$^{-/-}$ MEFs expressing PS2-T122R showed increased mitochondrial Ca^{2+} peaks compared to pre-depleted controls (Figure S4K). Note that the lack of PS2 effect on mitochondrial Ca^{2+} uptake in *Mfn2*$^{-/-}$ MEFs (Figure 3D) was not due to the morphological alterations of mitochondria induced by Mfn2 ablation, because *Mfn1*$^{-/-}$ MEFs showed an even more pronounced organelle fragmentation (Figure S4L). The PS2-dependent modulation of ER-mitochondria coupling also is independent of other MAM-associated proteins, such as DRP1 (Friedman et al., 2011; Figure S4M) or VDAC (Szabadkai et al., 2006; see below and Figure S6E).

We have demonstrated previously that endogenous PS2 also plays a constitutive role in modulating ER-mitochondria interplay (Zampese et al., 2011). Knockdown of endogenous PS2 (Figure 3E) by siRNA did not affect ER-mitochondria Ca^{2+} crosstalk in *Mfn2*$^{-/-}$ MEFs (Figure 3F) but decreased it in WT MEFs (Figure 3G). This result, in agreement with the morphological data (Figures S2A and S2B), indicates that endogenous PS2 also contributes to ER-mitochondrial juxtaposition, but only when Mfn2 is

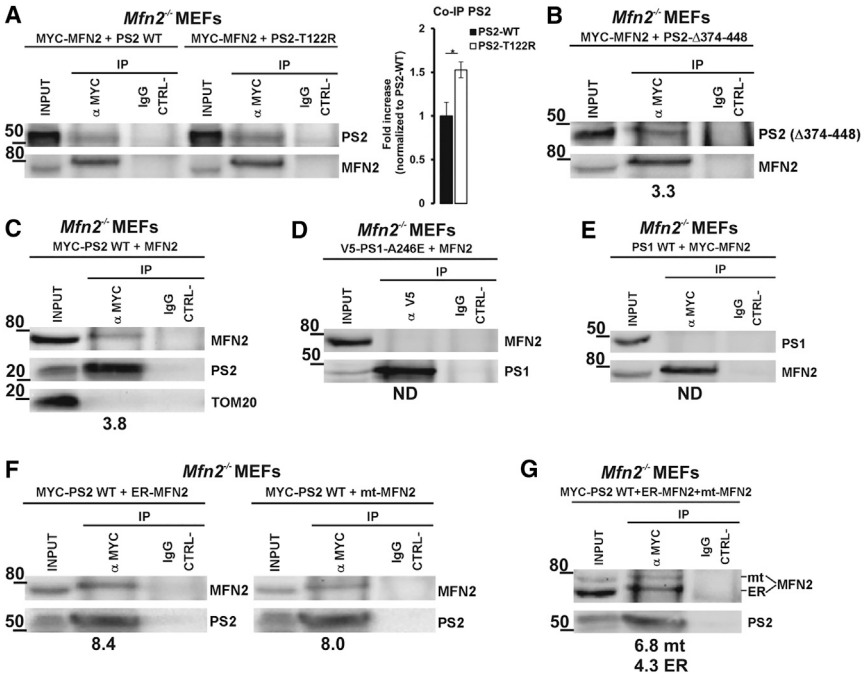

Figure 4. Selective Binding of PS2 and Mfn2

(A–G) *Mfn2*$^{-/-}$ MEFs co-expressing Myc-Mfn2 and PS2 (WT or T122R) (A), Myc-Mfn2 and PS2-Δ374-448 (B), Myc-PS2 WT and Mfn2 (C), V5-PS1-A246E and Mfn2 (D), PS1 WT and Myc-Mfn2 (E), and Myc-PS2 WT and either Mfn2IYFFT (ER-Mfn2) or Mfn2ActA (mt-Mfn2) (F) or both Mfn2 forms (G) were lysed and immunoprecipitated with different specific antibodies (anti-Myc or anti-V5, as indicated in each panel) or with irrelevant IgG, as a negative control (IgG CTRL−). Representative western blots of precipitates (IP) and total lysates (input) probed with specific antibodies for the indicated proteins are shown ($n \geq 3$ independent experiments per condition). (A) Bars on right represent the amounts of coIP PS2, either WT or T122R, normalized to those of the corresponding IP Mfn2. (B–G) At the bottom of each panel, the percentages of the specific coIP protein (B, PS2 Δ374–448; C, D, F, and G, Mfn2; (E, PS1), compared to its input, are reported (see the Supplemental Experimental Procedures). ND, not detectable. Linked to Figure S4.

also present. Indeed, when Mfn2 was re-expressed in *Mfn2*$^{-/-}$ MEFs (Figure 3E), PS2 silencing decreased ER-mitochondria Ca^{2+} transfer (Figure 3H). By a reciprocal approach, in MEFs deficient in both PS1 and PS2 (PS-DKO), Mfn2 knockdown did not affect cytosolic Ca^{2+} peaks but increased mitochondrial Ca^{2+} peaks compared to controls (Figure S5A, in agreement with the morphological data on ER-mitochondria physical tethering [Figure S2E]), as previously described in different cell lines (Filadi et al., 2015).

PS2 and Mfn2, but Not Their Homologs PS1 and Mfn1, Physically Interact

Immunoprecipitation (IP) assays in *Mfn2*$^{-/-}$ MEFs (and in SH-SY5Y cells; Figure S5B) expressing a Myc-tagged form of Mfn2 and either WT or mutated (T122R) PS2 (Figure 4A, left) indicated that Myc-Mfn2 co-immunoprecipitates with the full-length form of PS2 (and with higher efficiency in the presence of the mutated PS2-T122R form compared to the WT counterpart; Figure 4A, right). At lower molecular weights, a faint band corresponding to the C-terminal fragment of PS2 (which originates after PS maturation and incorporation into the γ-secretase complex [Haass and De Strooper, 1999]), also was revealed, whereas the PS2 N-terminal fragment (Haass and De Strooper, 1999) was never detected (Figure S5B). Moreover, Myc-Mfn2 still co-immunoprecipitated a truncated form of PS2 (PS2-Δ374–448; Figure 4B), lacking the final part of its C terminus (Figure S5C), thus restricting the Mfn2-interacting domain of PS2 to its large cytosolic loop. Because PS2-Δ374–448 contains also the loss-of-function mutation D366A, the ability of PS2 to bind Mfn2 is independent from its enzymatic activity (as demonstrated for other Ca^{2+}-related PS2 functions [Brunello et al., 2009; Zampese et al., 2011]).

By a reciprocal approach, in *Mfn2*$^{-/-}$ MEFs co-expressing Mfn2 and Myc-PS2, IP of Myc-PS2 pulled down Mfn2, but not another abundant OMM protein, Tom20 (Figure 4C). Moreover, the PS2 homolog PS1, which has been suggested to contribute to ER-mitochondria tethering in a fashion similar to PS2 (Area-Gomez et al., 2012), did not interact with Mfn2 in our assay. In *Mfn2*$^{-/-}$ MEFs overexpressing a tagged PS1 (V5-PS1), either WT or FAD-PS1-A246E, and Myc-Mfn2, anti-V5 (Figure 4D) or anti-Myc (Figure 4E) co-immunoprecipitations (coIPs) did not pull down Mfn2 or PS1, respectively. Moreover, in WT or *Mfn2*$^{-/-}$ MEFs co-expressing Mfn1 and PS2, PS2 did not immunoprecipitate Mfn1 (Figure S5D). Finally, the capability of endogenous PS2 and Mfn2 to physically interact was confirmed by IP experiments in crude mitochondrial fractions from mouse brain (see below and Figure 6C). Because PS2 is an integral ER membrane protein that is enriched in MAMs (Area-Gomez et al., 2009) and Mfn2 also is present in this location (de Brito and Scorrano, 2008), the two proteins could interact both in *cis* and/or in *trans*. IPs in *Mfn2*$^{-/-}$ MEFs expressing Myc-PS2 WT and the two Mfn2 mutants that are targeted to either the OMM (Mfn2ActA) or to ER membranes (Mfn2IYFFT) (de Brito and Scorrano, 2008) showed that PS2 pulls down either proteins separately (Figure 4F), or together, when the three proteins were co-expressed (Figure 4G).

The two proteins interact also in living cells: fluorescence recovery after photobleaching (FRAP) (Reits and Neefjes, 2001) experiments showed that the mobility within ER membranes of PS2 (but not of PS1) is modulated by Mfn2. Figure 5 shows representative confocal images of a *Mfn2*$^{-/-}$ MEF expressing CFP-PS2 (with a clear reticular ER pattern) before (Figure 5A) and after photobleaching (Figures 5B and 5C) and representative FRAP traces (Figures 5D–5F) of *Mfn2*$^{-/-}$ MEFs expressing CFP-PS1WT, CFP-PS2WT, or CFP-PS2-T122R alone or together with Mfn2. While Mfn2 co-expression did not affect fluorescence recovery of CFP-PS1WT (Figure 5D), in contrast it

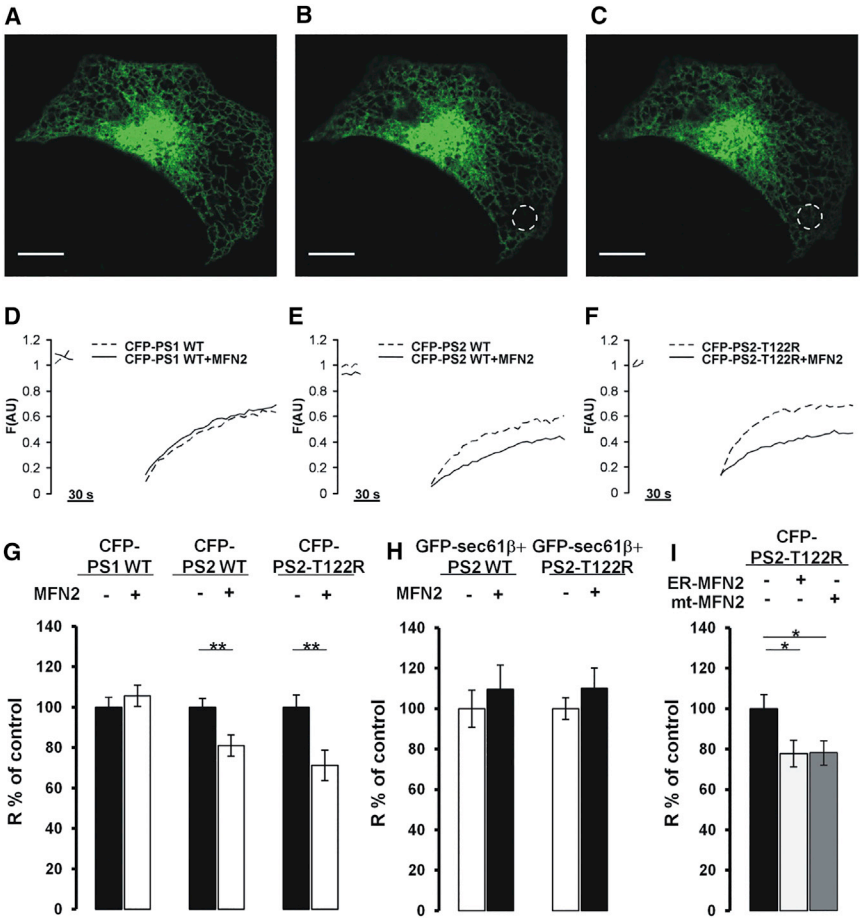

Figure 5. PS2, but Not PS1, Shows a Reduced Mobile Fraction upon Mfn2 Expression

(A–C) Representative confocal images show a *Mfn2*$^{-/-}$ MEF expressing CFP-PS2 before (A) and after (B and C) photobleaching in the drawn region of interest (ROI). Scale bar, 10 μm.

(D–F) Representative FRAP traces of CFP-PS1WT- (D), CFP-PS2WT- (E), or CFP-PS2-T122R- (F) expressing *Mfn2*$^{-/-}$ MEFs, with (continuous trace) or without (dotted trace) co-expression of Mfn2. Traces show fluorescence intensities before and after photobleaching for the indicated time. Fluorescence values were normalized to prebleached ones and plotted over time.

(G–I) Bars represent mean values of the mobile fraction of the indicated fluorescent protein (R) in the presence or absence of WT Mfn2 (G and H) or ER/mt-targeted Mfn2 (I). In (H), PS2 (WT or T122R) was co-expressed with the chimeric fluorescent protein GFP-sec61β. Mean ± SEM; n = 14–34 cells per condition, imaged in four independent experiments.

significantly reduced that of CFP-PS2WT (Figure 5E) or CFP-PS2-T122R (Figure 5F), with the greatest reduction for the latter. Accordingly, the mobile fraction (R) of fluorescent PS2, but not that of PS1, was reduced by Mfn2 co-expression, with PS2-T122R being the most affected (Figure 5G). FRAP analysis of cells expressing the chimeric ER protein GFP-sec61β (Shibata et al., 2008) and PS2 (WT or T122R), with or without Mfn2, indicated no significant difference in GFP-sec61β mobile fraction (Figure 5H), suggesting that the PS2-Mfn2 interaction does not alter ER membranes and its global membrane protein mobility. Moreover, the expression of one of the two Mfn2 mutants targeted to either the OMM (Mfn2ActA) or to ER membranes (Mfn2IYFFT) (de Brito and Scorrano, 2008), together with CFP-PS2-T122R (conditions that do not affect ER-mitochondria coupling; Figures S4G–S4J; Filadi et al., 2015) modified the mobility of CFP-PS2-T122R to a similar extent (Figure 5I) as that induced by WT Mfn2 (Figure 5G). For all the different conditions tested, the diffusion constant *D* (see the Experimental Procedures) also was calculated but it was unchanged (Table S2).

Altogether these findings exclude a possible PS2 mobility interference due to differential organelles' apposition, and they suggest that the observed reduction in PS2 mobile fraction in the presence of Mfn2 is due to their physical interaction.

FAD-PS2 Accumulates in MAMs, Favoring Its Binding to Mfn2

ER-mitochondria contacts are thought to occur in MAMs. To verify whether the different ER-mitochondria tethering efficacy of WT and FAD-PS2 could depend on their differential MAM localization, we used brain homogenates from WT and FAD-PS2 transgenic (Tg) mice (carrying the PS2 mutation N141I [Kipanyula et al., 2012]). PS2 was present both in the generic ER/microsome fraction as well as in MAMs (Figure 6A). PS2 appeared to be present in similar amounts in MAMs and microsomes of WT mice, but it was enriched 2.2-fold in MAMs of FAD-PS2 Tg mice compared to total ER membranes (Figure 6B). In addition, Mfn2 immunoprecipitates from crude mitochondrial fractions of Tg mice brains contained more PS2 than those from WT mice (Figures 6C and 6D). This further suggests that the PS2 mutant is more enriched than the WT form in the fraction of ER membranes that contaminates crude mitochondria (ER-MAMs; visible also from the input lanes of Figure 6C), and thus its binding to Mfn2 is favored.

ER-mitochondria tethering is likely not assured by a single type of tether, and, if one structure is ablated, a compensatory increase of another may occur. The IP3R/GRP75/VDAC complex has been suggested to contribute to ER-mitochondria coupling (Szabadkai et al., 2006). Thus, another way through which PS2 increases ER-mitochondria tethering could be by promoting IP3R/GRP75/VDAC complex formation. However, the expression levels of the three proteins in MEF cells were not affected by PS2-T122R expression or Mfn2 ablation (Figures S6A and S6B). Moreover, GRP75 and VDAC1 levels in the MAM fractions of PS2-N141I Tg mice brains were comparable to those of WT mice (Figure 6E). Furthermore, PS2-T122R expression in WT MEFs or Mfn2 ablation slightly reduced the IP3R3-mediated

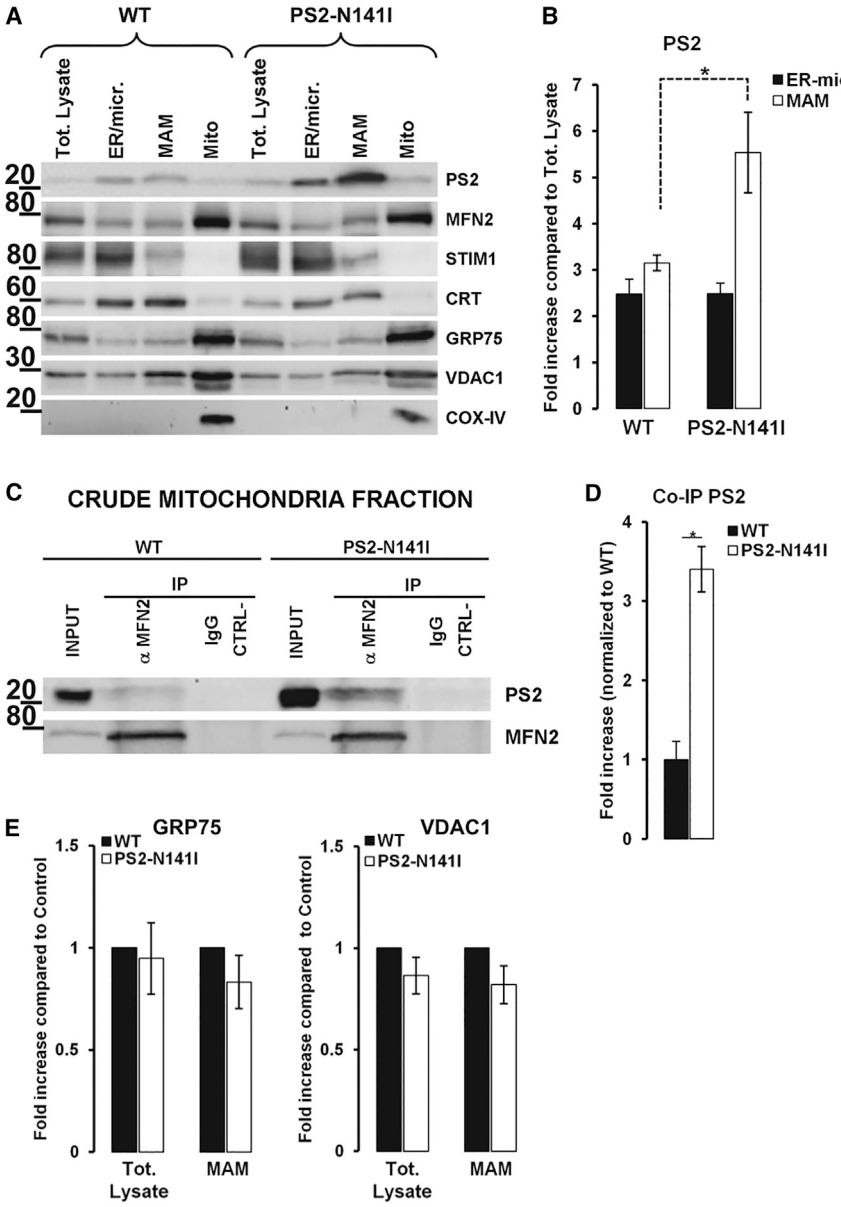

Figure 6. PS2 and Mfn2 Are Enriched in Brain MAMs of FAD-PS2N141I Tg Mice

(A) Representative western blot of the indicated proteins in brain subcellular fractions (35 μg/lane) from WT and FAD-PS2-N141I Tg mice is shown (n = 4 western blots of three independent preparations). Tot. lysate, total brain homogenates; ER/micr., microsomes; MAM, mitochondria-associated membranes; Mito, pure mitochondria. Markers for subcellular fractions are as follows: STIM1 and CRT (ER), GRP75 and VDAC1 (MAM/mitochondria), and COX-IV (mitochondria).

(B) Bars represent relative fold increase, compared to total brain homogenates, of PS2 abundance in ER and MAM fractions of WT and PS2-N141I Tg mice (mean ± SEM; n = 4 independent experiments).

(C) Representative (n = 4) western blot of crude mitochondrial fractions from brains of WT and FAD-PS2-N141I Tg mice immunoprecipitated with Mfn2-specific antibodies, or with irrelevant IgG as a negative control (IgG CTRL−). Precipitated (IP) and total crude mitochondrial fractions (input) were probed with PS2-specific antibodies.

(D) Bars represent relative fold increase, compared to WT, of PS2 abundance co-precipitated with Mfn2 in crude mitochondrial fractions from brain of PS2-N141I Tg mice, in experiments as in (C) (mean ± SEM; n = 4 independent experiments from three independent preparations).

(E) Bars represent relative fold increase, compared to WT, of GRP75 (left) or VDAC1 (right) abundance in total lysate or MAM fraction obtained from FAD-PS2-N141I Tg mice brains, as in (A) (mean ± SEM; n = 4). Linked to Figure S5.

GRP75 coIP (Figures S6C and S6D), suggesting that neither PS2 expression nor Mfn2 ablation increased IP3R3-GRP75 interaction. Finally, in MEF cells KO for VDAC 1 and 3 (*VDAC1/3*$^{-/-}$ MEFs [Chiara et al., 2008]), the functional potentiating effect of PS2-T122R on ER-mitochondria Ca^{2+} transfer was still observed (Figure S6E), further suggesting a marginal role for the IP3R/GRP75/VDAC complex in the PS2 effect here investigated.

Human FAD-PS2 Fibroblasts Show Increased ER-Mitochondria Tethering and Ca^{2+} Crosstalk

It could be argued that the present findings and those obtained in previous works (Kipanyula et al., 2012; Zampese et al., 2011) have been obtained mainly in PS2-overexpressing cells. To address this criticism, Ca^{2+} responses were analyzed in human fibroblasts from a FAD patient carrying the PS2-N141I mutation and a healthy control (matched for age and sex) expressing cytosolic or mitochondria-targeted aequorin (typical experiment shown in Figure 7A). Upon stimulation with the IP_3-generating agonist bradykinin, FAD-PS2 fibroblasts showed reduced cytosolic and mitochondrial Ca^{2+} peaks compared to controls. When the amplitude of cytosolic Ca^{2+} peaks in control fibroblasts was reduced to match that of FAD-PS2 fibroblasts, the mitochondrial Ca^{2+} peaks in the latter were larger than those of pre-depleted controls (Figure 7B). As shown in other cell types (Zampese et al., 2011), the increased mitochondrial Ca^{2+} peaks were not due to a direct effect of FAD-PS2 on the mitochondrial Ca^{2+} uptake machinery, because control and FAD-PS2 fibroblasts showed comparable $[Ca^{2+}]_m$ increases upon permeabilization and perfusion with different intracellular-like media at fixed Ca^{2+} concentrations (Figure 7C). Similar results were obtained measuring cytosolic and mitochondrial Ca^{2+} peaks in single cells by two GFP-based Ca^{2+} indicators (Figure 7D): the mitochondrial 4mtD1cpv and the nuclear H2BD1cpv (as a surrogate to monitor cytosolic Ca^{2+} [Giacomello et al., 2010; Zampese et al., 2011]). For increases in nuclear Ca^{2+} in the same range (0.2–0.55 $nuc\Delta R/R_0$), the mitochondrial responses

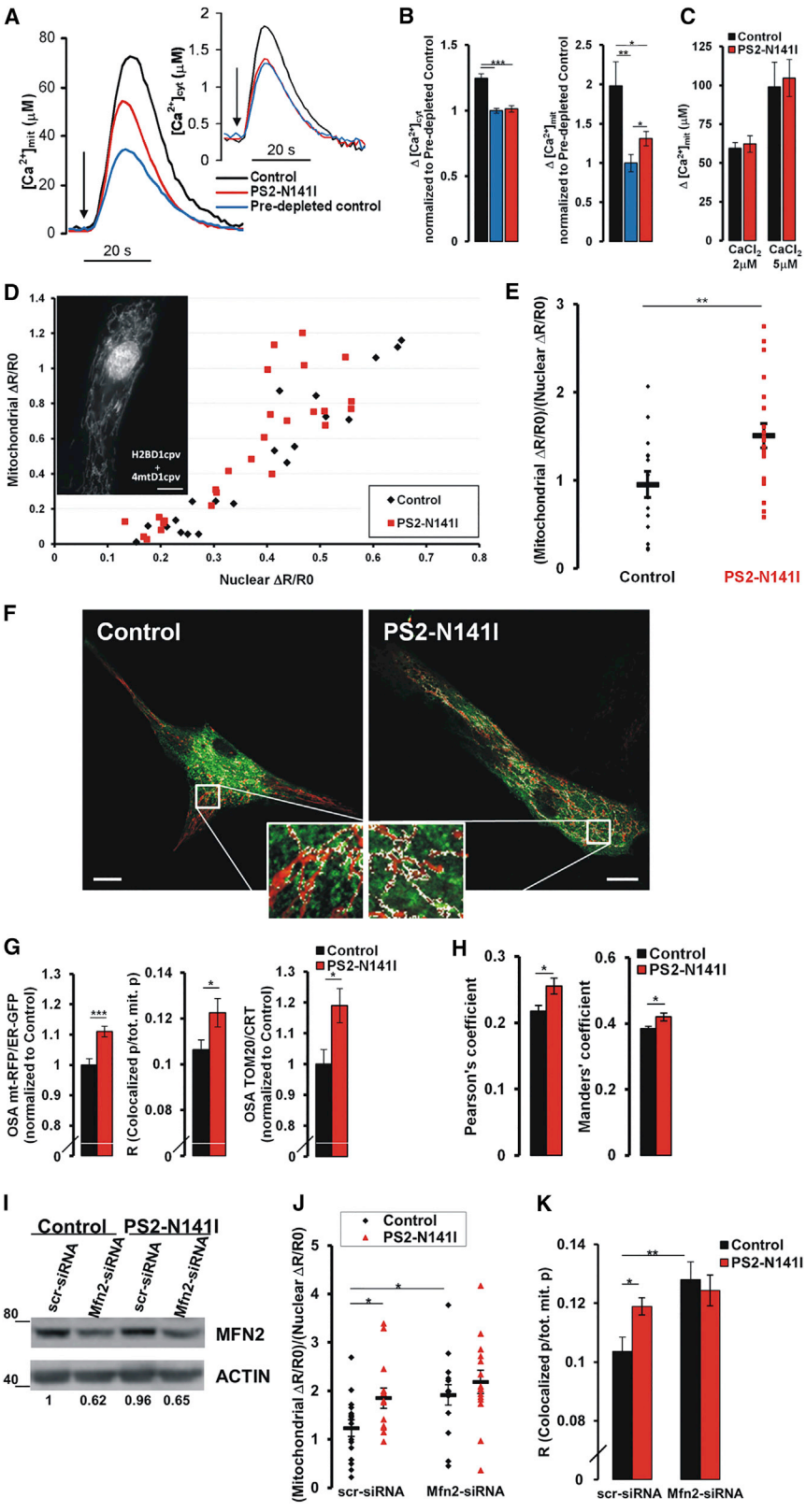

Figure 7. FAD-PS2 Human Fibroblasts Show Increased ER-Mitochondria Coupling

(A) Representative cytosolic (inset) and mitochondrial Ca^{2+} traces in control (black), pre-depleted control (blue), and FAD-PS2-N141I (red) fibroblasts, bathed in Ca^{2+}-free, EGTA-containing medium and challenged with 100 nM BK (where indicated by the arrow), are shown.

(B) Bars represent mean $[Ca^{2+}]_{cyt}$ (left) and $[Ca^{2+}]_{mit}$ (right) peaks upon stimulation in the different conditions (mean ± SEM; n = 4–14 independent experiments).

(C) Bars represent mean $[Ca^{2+}]_{mit}$ peaks in control and FAD-PS2-N141I fibroblasts expressing mit-Aeq upon cell permeabilization and perfusion with the indicated $[CaCl_2]$ (see the Experimental Procedures; mean ± SEM; n = 4 independent experiments).

(D) $[Ca^{2+}]_{mit}$ and nuclear Ca^{2+} ($[Ca^{2+}]_{nuc}$) peaks in single control and FAD fibroblasts, as revealed by specific cameleon Ca^{2+} probes. Fibroblasts co-expressing H2BD1cpv and 4mtD1cpv (inset) were stimulated as described in (A). The increase in $[Ca^{2+}]_{mit}$ (mitochondrial $\Delta R/R_0$) is plotted as a function of the corresponding increase in $[Ca^{2+}]_{nuc}$ (nuclear $\Delta R/R_0$) in the same cell. Each symbol represents one cell; cells were imaged in three independent experiments.

(E) Plot of the ratio between mitochondrial and nuclear peak values is shown, measured as described in (D) within the nuclear 0.2–0.55 $\Delta R/R_0$ interval in control and FAD-PS2 fibroblasts (n = 21 FAD cells and 15 control cells imaged in three independent experiments; mean ± SEM).

(F) Representative confocal images of control and FAD-PS2-N141I fibroblasts co-expressing mt-RFP and ER-GFP. White pixels indicates ER-mitochondria co-localization. Scale bar, 10 μm.

(G) Overlapping surface area (OSA) or perimeter coefficient (R) quantification is shown, calculated from single confocal images as in (F), for mt-RFP/ER-GFP (left and middle) or TOM20/CRT immunofluorescence (right) (mean ± SEM; n = 44–63 fibroblasts expressing mt-RFP/ER-GFP, imaged in four independent experiments; n = 23–28 cells stained by immunofluorescence, imaged in three independent experiments).

(H) Bars represent co-localization indexes (Pearson's and Manders'), calculated from entire single confocal images as in (F), for control and FAD-PS2-N141I fibroblasts (mean ± SEM).

(I) Representative (n = 3 for each condition) western blot of protein lysates from control and FAD-PS2-N141I fibroblasts is shown, transfected as indicated and probed with specific antibodies for the indicated proteins.

(J) Plot of the ratio between mitochondrial and nuclear Ca^{2+} peak values is shown, upon BK stimulation, measured as described in (E) in control and FAD-PS2 fibroblasts transfected with scramble (scr-siRNA) or Mfn2-specific (Mfn2-siRNA) siRNAs (n = 12–16 cells for each conditions imaged in three independent experiments; mean ± SEM).

(K) Perimeter coefficient (R) quantification is shown, calculated from single confocal images as in (F), for mt-RFP/ER-GFP in control and FAD-PS2 fibroblasts transfected as in (J) (mean ± SEM; n = 15–21 cells for each condition, imaged in three independent experiments).

of FAD-PS2 fibroblasts were significantly larger than those of control fibroblasts (Figure 7E).

As in FAD-PS2-overexpressing cells (Zampese et al., 2011) and neurons from FAD-PS2 Tg mice (Kipanyula et al., 2012), in human FAD-PS2 fibroblasts expressing a mt-RFP and an ER-GFP (Figure 7F), different co-localization coefficients (see the Experimental Procedures) were significantly increased compared to controls (Figures 7G, left, and 7H), indicating closer interactions between mitochondria and ER that could account for the different efficacy of ER-mitochondria Ca^{2+} crosstalk. Similar results were obtained measuring the signal co-localization of two immunolabelled endogenous markers, the ER protein calreticulin and the mitochondrial protein Tom20 (Figure 7G, right).

Importantly, also in human FAD-PS2 fibroblasts, the reinforcing effect on ER-mitochondria coupling depends on the presence of Mfn2: upon Mfn2 knockdown by specific siRNA (Figure 7I), the potentiating effect of FAD-PS2-N141I mutant on Ca^{2+} transfer between ER and mitochondria (Figure 7J), as well as on their physical apposition (Figure 7K), was dampened, and no significant difference between control and FAD-PS2-N141I fibroblasts was observed.

DISCUSSION

The correct organization and the dynamic interactions between ER and mitochondria, and especially their Ca^{2+} crosstalk, coordinate and modulate key aspects of cell physiology, death, and survival (Contreras et al., 2010; de Brito and Scorrano, 2010; Filadi et al., 2012). We have described that PS2, but not PS1, is able to modulate ER-mitochondria coupling (Zampese et al., 2011), although the molecular mechanism of this phenomenon has not been clarified yet. By crossed genetic complementation and ablation experiments, we here show that, in order to modulate ER-mitochondria coupling, PS2 requires the expression of Mfn2. Functional and biochemical evidence indicates that PS2 (WT and FAD), by interacting, likely via its big cytosolic loop, with Mfn2 at both sides of MAM domains, induces an increase of ER-mitochondria vicinity and favors their Ca^{2+} transfer. In contrast, PS1 and Mfn1 (as well as other mitochondria-associated proteins, such as DRP1 and VDAC) are not involved in this interplay of molecules/organelles.

Although PS2 and Mfn2 work in tandem to modulate ER-mitochondria coupling, for other cellular functions, the two proteins are independent. The previously described PS2 effect on ER Ca^{2+} content (Brunello et al., 2009; Giacomello et al., 2005; Zatti et al., 2004, 2006), for example, is Mfn2 independent, and it is more strongly affected when PS2 is not engaged in Mfn2 binding, such as in *Mfn2*$^{-/-}$ MEFs. Along the same line, the Mfn-mediated effect on mitochondria fusion (Chen et al., 2003) seems to be PS2 independent. Thus, both proteins show distinct and multiple roles, some similar to those exerted also by their homolog proteins (PS1 and Mfn1, respectively) and others completely divergent.

Our findings shed insight into the key issue of ER-mitochondria connection and the mechanism of their juxtaposition. Although the molecular composition of the tethering structures in mammals remains elusive, the present data provide important information. In addition to the demonstration that Mfn2 does not play a positive role in the formation of tethering complexes, as the close apposition between the two organelles is conserved, and actually increased, upon Mfn2 ablation/depletion (Cosson et al., 2012; Filadi et al., 2015; Li et al., 2015; Wang et al., 2015), we show that the PS2 ability to enforce organelles' coupling is strictly Mfn2 dependent, whereas the protein works independently of the IP3R/GRP75/VDAC complex. On the contrary, Mfn2 is able to exert its inhibitory activity on tethering even in the absence of PS2, although the abundance of the latter modulates this outcome.

Based on these experimental data, we propose a revised model for ER-mitochondria juxtaposition, in which increased tethering between the two organelles is caused either by Mfn2 depletion or by its binding to PS2 (or potentially other proteins capable of physically interacting with Mfn2) that, by sequestering it both in *cis* and in *trans*, removes Mfn2 inhibition at both OMM and ER membranes and allows the different molecular components to assemble and build the functional tether (Figure S7). Notably, our data indicate that the simultaneous presence of Mfn2 on both ER and mitochondria is necessary to impair ER-mitochondria juxtaposition, suggesting that the proper assembly of tether structures can be efficiently inhibited only when both ER and mitochondrial components are blocked by Mfn2. Whether PS2 is also one of the molecules forming the tether complex or if it works as a pure bait for the stumbling block Mfn2 remains to be investigated; however, our FRAP data suggest this latter explanation to be the most likely. Indeed, the mobility of CFP-PS2 in living cells is equally altered by the presence of WT Mfn2 (which decreases ER-mitochondria tethering) or its forms individually expressed only on the ER or mitochondria membranes (which are not able to modify organelles' tethering), thus suggesting that PS2 likely binds only to Mfn2 and not to tether structures.

In addition to the above-described role, PS2, when mutated, is responsible for FAD. We here demonstrate that, in human fibroblasts bearing the PS2-N141I mutation, ER-mitochondria coupling is increased compared to controls. From the mechanistic point of view, the most important finding is that this feature is similarly affected by FAD-PS2, both quantitatively and qualitatively, in transiently or stably overexpressing AD models (Kipanyula et al., 2012; Zampese et al., 2011) and in cells from an FAD patient.

Concerning the molecular mechanism through which FAD-linked PS2 mutants are more efficient than their WT counterpart at modulating ER-mitochondria coupling, our results indicate that both WT and FAD-PS2 bind to Mfn2 and need its presence to increase the tethering. However, while IP and FRAP experiments exclude a possible interaction with PS1, our data show that FAD-PS2 mutants are more enriched in MAMs than the WT form, bind more Mfn2 by interacting with it both in *cis* and in *trans*, and thus form more PS2-Mfn2 complexes. These latter are critical for releasing the stumbling block exerted by Mfn2 on different molecular components, facilitating the formation of ER-mitochondria tether structures (Figure S7).

The mechanism by which FAD mutants preferentially localize in MAMs within ER membranes, compared to the WT form, might be multiple, such as PS2 conformation (full-length or processed

form), differential post-translational protein modifications (for example, palmitoylation or ubiquitination, as shown for other MAM proteins [Lynes et al., 2012; Sugiura et al., 2013]), or interactions with other anchor molecules. Additional investigation is required to clarify this point.

From a functional point of view, the increased ER-mitochondria coupling induced by FAD-PS2 expression could have different and important consequences. For example, the strengthened organelles' Ca^{2+} crosstalk, under certain conditions and over long periods of time, may alter bioenergetics functions and/or increase mitochondria-dependent cell death (Contreras et al., 2010; Pizzo et al., 2012). Moreover, ER-mitochondria interplay can influence mitochondrial network shaping and dynamics (Friedman et al., 2011; Korobova et al., 2013), as well as neuronal organelle transport (Chang et al., 2011; MacAskill and Kittler, 2010). Indeed, an alteration in MAM composition (Hedskog et al., 2013) and a variety of mitochondrial dysfunctions, such as unbalanced fission and fusion (Wang et al., 2009), metabolic defects (Swerdlow et al., 2010), or altered organelle distribution in neurons (Su et al., 2010), have been described in AD, as well as in normal brain aging (Lin and Beal, 2006; Toescu and Verkhratsky, 2004).

Thus, in the case of AD-linked PS2 mutants, ER-mitochondria interplay and organelles' alterations may represent a direct effect of the mutated protein, and, accordingly, these forms of FAD may be included, together with Parkinson's disease (Haelterman et al., 2014), amyotrophic lateral sclerosis (Stoica et al., 2014), and Huntington's disease (Chakraborty et al., 2014), in the long list of neurological disorders with modified ER-mitochondria connections and primary mitochondrial dysfunctions (Calì et al., 2012; Celsi et al., 2009).

EXPERIMENTAL PROCEDURES

Animal Handling and Care

The transgenic mouse line PS2.30H (expressing PS2-N141I) was kindly donated by Dr. L. Ozmen (F. Hoffmann-La Roche). It has the background strain of C57BL/6 mice, which was used as a WT control and was purchased from Charles River. All procedures were carried out in strict adherence to the Italian regulations on animal protection and care and with the explicit approval of the local veterinary authority (CEASA no. 56880).

Cell Culture, Plasmids, and Transfection

Different cell types (human fibroblasts, MEFs, and SH-SY5Y) were grown and transfected with the indicated plasmids, as detailed in the Supplemental Experimental Procedures.

Confocal Analysis and FRAP Experiments

Cells expressing different fluorescent proteins were imaged with a Leica SP5 confocal system (DM IRE2). Co-localization and FRAP analysis were performed as detailed in the Supplemental Experimental Procedures.

EM Analysis

Conventional EM was carried out as described in the Supplemental Experimental Procedures using a Fei Tecnai 12 BioTwin Spirit transmission electron microscope.

Ca^{2+} Measurements and Fluorescence Imaging

MEFs and human fibroblasts expressing either aequorin Ca^{2+} probes or Ca^{2+} fluorescent probes (H2BD1cpv, 4mtD1cpv, and ERD4) were analyzed as previously described (Zampese et al., 2011) and detailed in the Supplemental Experimental Procedures.

Subcellular Fractionation, Preparation of Protein Extracts, IP Assay, and Western Blot Analysis

For subcellular fractionation, mouse brains from adult C57B6/J WT or FAD-PS2-N141I Tg mice (Kipanyula et al., 2012) were homogenized using a Teflon pestle. The different fractions were obtained from the homogenate essentially as detailed in the Supplemental Experimental Procedures.

For conventional western blot analysis, 35 μg protein extracts prepared as described in the Supplemental Experimental Procedures were loaded onto polyacrylamide gels (10%–12%) and immunoblotted with specific antibodies.

For IP, cells were harvested and solubilized in modified radio-immunoprecipitation assay (RIPA) buffer (see the Supplemental Experimental Procedures), and 300 μg protein extracts were incubated with the indicated antibodies on a rocker platform at 4°C as detailed in the Supplemental Experimental Procedures.

Materials

All the materials were purchased from Sigma-Aldrich, except ionomycin (Calbiochem) and restriction/modification enzymes (New England Biolabs).

Statistical Analysis

All data are representative of at least three different experiments. Data were analyzed with Origin 7.5 SR5 (OriginLab) and ImageJ (NIH). Numerical values presented throughout the text refer to mean ± SEM (n = number of independent experiments or cells; *$p < 0.05$, **$p < 0.01$, and ***$p < 0.001$, unpaired Student's t test for normally distributed data or Wilcoxon rank-sum test).

SUPPLEMENTAL INFORMATION

Supplemental Information includes Supplemental Experimental Procedures, seven figures, and two tables and can be found with this article online at http://dx.doi.org/10.1016/j.celrep.2016.05.013.

AUTHOR CONTRIBUTIONS

R.F. performed all biochemical and calcium experiments as well as data analysis. E.G. performed PS molecular cloning and FRAP experiments. G.T. and A.L. performed EM analysis. P.P. conceived the study and designed the experiments. R.F., T.P., and P.P. wrote the paper.

ACKNOWLEDGMENTS

We thank L. Scorrano for all Mfn-MEF lines and the different Mfn cDNAs, B. De Strooper for WT and PS-DKO MEFs, A. Rasola for WT and *VDAC1/3*$^{-/-}$ MEFs, and G.K. Voeltz for the cDNAs encoding GFP-sec61β. We are grateful to M. Bortolozzi for his help in FRAP analysis; A.C. Frigo for her statistical advice; P. Magalhães for critically revising the manuscript; and E. Zampese, C. Fasolato, and D. Pendin for valuable discussions and scientific support. This work was funded by grants from the Italian Ministry of University and Scientific Research to T.P. and P.P., Fondazione Cassa di Risparmio di Padova e Rovigo (CARIPARO Foundation; Progetti d'eccellenza 2011/2012) and EU Joint Programme-Neurodegenerative Disease Research to P.P. and the Veneto Region, the Italian Institute of Technology, the Strategic Projects of the University of Padua, and the Italian National Research Council to T.P.

Received: December 14, 2015
Revised: March 23, 2016
Accepted: April 28, 2016
Published: May 26, 2016

REFERENCES

Area-Gomez, E., de Groof, A.J., Boldogh, I., Bird, T.D., Gibson, G.E., Koehler, C.M., Yu, W.H., Duff, K.E., Yaffe, M.P., Pon, L.A., and Schon, E.A. (2009). Presenilins are enriched in endoplasmic reticulum membranes associated with mitochondria. Am. J. Pathol. *175*, 1810–1816.

Area-Gomez, E., Del Carmen Lara Castillo, M., Tambini, M.D., Guardia-Laguarta, C., de Groof, A.J., Madra, M., Ikenouchi, J., Umeda, M., Bird, T.D., Sturley, S.L., and Schon, E.A. (2012). Upregulated function of mitochondria-associated ER membranes in Alzheimer disease. EMBO J. *31*, 4106–4123.

Bionda, C., Portoukalian, J., Schmitt, D., Rodriguez-Lafrasse, C., and Ardail, D. (2004). Subcellular compartmentalization of ceramide metabolism: MAM (mitochondria-associated membrane) and/or mitochondria? Biochem. J. *382*, 527–533.

Bravo, R., Vicencio, J.M., Parra, V., Troncoso, R., Munoz, J.P., Bui, M., Quiroga, C., Rodriguez, A.E., Verdejo, H.E., Ferreira, J., et al. (2011). Increased ER-mitochondrial coupling promotes mitochondrial respiration and bioenergetics during early phases of ER stress. J. Cell Sci. *124*, 2143–2152.

Brunello, L., Zampese, E., Florean, C., Pozzan, T., Pizzo, P., and Fasolato, C. (2009). Presenilin-2 dampens intracellular Ca^{2+} stores by increasing Ca^{2+} leakage and reducing Ca^{2+} uptake. J. Cell. Mol. Med. *13* (*9B*), 3358–3369.

Calì, T., Ottolini, D., and Brini, M. (2012). Mitochondrial Ca(2+) and neurodegeneration. Cell Calcium *52*, 73–85.

Cárdenas, C., Miller, R.A., Smith, I., Bui, T., Molgó, J., Müller, M., Vais, H., Cheung, K.H., Yang, J., Parker, I., et al. (2010). Essential regulation of cell bioenergetics by constitutive InsP3 receptor Ca2+ transfer to mitochondria. Cell *142*, 270–283.

Celsi, F., Pizzo, P., Brini, M., Leo, S., Fotino, C., Pinton, P., and Rizzuto, R. (2009). Mitochondria, calcium and cell death: a deadly triad in neurodegeneration. Biochim. Biophys. Acta *1787*, 335–344.

Chakraborty, J., Rajamma, U., and Mohanakumar, K.P. (2014). A mitochondrial basis for Huntington's disease: therapeutic prospects. Mol. Cell. Biochem. *389*, 277–291.

Chang, K.T., Niescier, R.F., and Min, K.T. (2011). Mitochondrial matrix Ca2+ as an intrinsic signal regulating mitochondrial motility in axons. Proc. Natl. Acad. Sci. USA *108*, 15456–15461.

Chen, H., Detmer, S.A., Ewald, A.J., Griffin, E.E., Fraser, S.E., and Chan, D.C. (2003). Mitofusins Mfn1 and Mfn2 coordinately regulate mitochondrial fusion and are essential for embryonic development. J. Cell Biol. *160*, 189–200.

Chiara, F., Castellaro, D., Marin, O., Petronilli, V., Brusilow, W.S., Juhaszova, M., Sollott, S.J., Forte, M., Bernardi, P., and Rasola, A. (2008). Hexokinase II detachment from mitochondria triggers apoptosis through the permeability transition pore independent of voltage-dependent anion channels. PLoS ONE *3*, e1852.

Contreras, L., Drago, I., Zampese, E., and Pozzan, T. (2010). Mitochondria: the calcium connection. Biochim. Biophys. Acta *1797*, 607–618.

Cosson, P., Marchetti, A., Ravazzola, M., and Orci, L. (2012). Mitofusin-2 independent juxtaposition of endoplasmic reticulum and mitochondria: an ultrastructural study. PLoS ONE *7*, e46293.

Csordás, G., Renken, C., Várnai, P., Walter, L., Weaver, D., Buttle, K.F., Balla, T., Mannella, C.A., and Hajnóczky, G. (2006). Structural and functional features and significance of the physical linkage between ER and mitochondria. J. Cell Biol. *174*, 915–921.

Csordás, G., Várnai, P., Golenár, T., Roy, S., Purkins, G., Schneider, T.G., Balla, T., and Hajnóczky, G. (2010). Imaging interorganelle contacts and local calcium dynamics at the ER-mitochondrial interface. Mol. Cell *39*, 121–132.

de Brito, O.M., and Scorrano, L. (2008). Mitofusin 2 tethers endoplasmic reticulum to mitochondria. Nature *456*, 605–610.

de Brito, O.M., and Scorrano, L. (2010). An intimate liaison: spatial organization of the endoplasmic reticulum-mitochondria relationship. EMBO J. *29*, 2715–2723.

Filadi, R., Zampese, E., Pozzan, T., Pizzo, P., and Fasolato, C. (2012). Endoplasmic reticulum-mitochondria connection, calcium cross-talk and cell fate: a closer inspection. In Endoplasmic Reticulum Stress in Health and Disease, P. Agostinis and A. Samali, eds. (Dordrecht, Heidelberg, New York, London: Springer), pp. 75–106.

Filadi, R., Greotti, E., Turacchio, G., Luini, A., Pozzan, T., and Pizzo, P. (2015). Mitofusin 2 ablation increases endoplasmic reticulum-mitochondria coupling. Proc. Natl. Acad. Sci. USA *112*, E2174–E2181.

Friedman, J.R., Lackner, L.L., West, M., DiBenedetto, J.R., Nunnari, J., and Voeltz, G.K. (2011). ER tubules mark sites of mitochondrial division. Science *334*, 358–362.

Giacomello, M., Barbiero, L., Zatti, G., Squitti, R., Binetti, G., Pozzan, T., Fasolato, C., Ghidoni, R., and Pizzo, P. (2005). Reduction of Ca^{2+} stores and capacitative Ca^{2+} entry is associated with the familial Alzheimer's disease presenilin-2 T122R mutation and anticipates the onset of dementia. Neurobiol. Dis. *18*, 638–648.

Giacomello, M., Drago, I., Bortolozzi, M., Scorzeto, M., Gianelle, A., Pizzo, P., and Pozzan, T. (2010). Ca^{2+} hot spots on the mitochondrial surface are generated by Ca^{2+} mobilization from stores, but not by activation of store-operated Ca^{2+} channels. Mol. Cell *38*, 280–290.

Glancy, B., and Balaban, R.S. (2012). Role of mitochondrial Ca2+ in the regulation of cellular energetics. Biochemistry *51*, 2959–2973.

Goedert, M., and Spillantini, M.G. (2006). A century of Alzheimer's disease. Science *314*, 777–781.

Haass, C., and De Strooper, B. (1999). The presenilins in Alzheimer's disease–proteolysis holds the key. Science *286*, 916–919.

Haelterman, N.A., Yoon, W.H., Sandoval, H., Jaiswal, M., Shulman, J.M., and Bellen, H.J. (2014). A mitocentric view of Parkinson's disease. Annu. Rev. Neurosci. *37*, 137–159.

Hamasaki, M., Furuta, N., Matsuda, A., Nezu, A., Yamamoto, A., Fujita, N., Oomori, H., Noda, T., Haraguchi, T., Hiraoka, Y., et al. (2013). Autophagosomes form at ER-mitochondria contact sites. Nature *495*, 389–393.

Hayashi, T., Rizzuto, R., Hajnoczky, G., and Su, T.P. (2009). MAM: more than just a housekeeper. Trends Cell Biol. *19*, 81–88.

Hedskog, L., Pinho, C.M., Filadi, R., Rönnbäck, A., Hertwig, L., Wiehager, B., Larssen, P., Gellhaar, S., Sandebring, A., Westerlund, M., et al. (2013). Modulation of the endoplasmic reticulum-mitochondria interface in Alzheimer's disease and related models. Proc. Natl. Acad. Sci. USA *110*, 7916–7921.

Hoppins, S., Lackner, L., and Nunnari, J. (2007). The machines that divide and fuse mitochondria. Annu. Rev. Biochem. *76*, 751–780.

Huang, P., Yu, T., and Yoon, Y. (2007). Mitochondrial clustering induced by overexpression of the mitochondrial fusion protein Mfn2 causes mitochondrial dysfunction and cell death. Eur. J. Cell Biol. *86*, 289–302.

Kipanyula, M.J., Contreras, L., Zampese, E., Lazzari, C., Wong, A.K., Pizzo, P., Fasolato, C., and Pozzan, T. (2012). Ca2+ dysregulation in neurons from transgenic mice expressing mutant presenilin 2. Aging Cell *11*, 885–893.

Kornmann, B., Currie, E., Collins, S.R., Schuldiner, M., Nunnari, J., Weissman, J.S., and Walter, P. (2009). An ER-mitochondria tethering complex revealed by a synthetic biology screen. Science *325*, 477–481.

Korobova, F., Ramabhadran, V., and Higgs, H.N. (2013). An actin-dependent step in mitochondrial fission mediated by the ER-associated formin INF2. Science *339*, 464–467.

Li, L., Gao, G., Shankar, J., Joshi, B., Foster, L.J., and Nabi, I.R. (2015). p38 MAP kinase-dependent phosphorylation of the Gp78 E3 ubiquitin ligase controls ER-mitochondria association and mitochondria motility. Mol. Biol. Cell *26*, 3828–3840.

Lin, M.T., and Beal, M.F. (2006). Mitochondrial dysfunction and oxidative stress in neurodegenerative diseases. Nature *443*, 787–795.

Lynes, E.M., Bui, M., Yap, M.C., Benson, M.D., Schneider, B., Ellgaard, L., Berthiaume, L.G., and Simmen, T. (2012). Palmitoylated TMX and calnexin target to the mitochondria-associated membrane. EMBO J. *31*, 457–470.

MacAskill, A.F., and Kittler, J.T. (2010). Control of mitochondrial transport and localization in neurons. Trends Cell Biol. *20*, 102–112.

Marchi, S., Patergnani, S., and Pinton, P. (2014). The endoplasmic reticulum-mitochondria connection: one touch, multiple functions. Biochim. Biophys. Acta *1837*, 461–469.

Pizzo, P., Drago, I., Filadi, R., and Pozzan, T. (2012). Mitochondrial Ca^{2+} homeostasis: mechanism, role, and tissue specificities. Pflugers Arch. *464*, 3–17.

Raturi, A., and Simmen, T. (2013). Where the endoplasmic reticulum and the mitochondrion tie the knot: the mitochondria-associated membrane (MAM). Biochim. Biophys. Acta *1833*, 213–224.

Reits, E.A., and Neefjes, J.J. (2001). From fixed to FRAP: measuring protein mobility and activity in living cells. Nat. Cell Biol. *3*, E145–E147.

Rojo, M., Legros, F., Chateau, D., and Lombès, A. (2002). Membrane topology and mitochondrial targeting of mitofusins, ubiquitous mammalian homologs of the transmembrane GTPase Fzo. J. Cell Sci. *115*, 1663–1674.

Rowland, A.A., and Voeltz, G.K. (2012). Endoplasmic reticulum-mitochondria contacts: function of the junction. Nat. Rev. Mol. Cell Biol. *13*, 607–625.

Rusiñol, A.E., Cui, Z., Chen, M.H., and Vance, J.E. (1994). A unique mitochondria-associated membrane fraction from rat liver has a high capacity for lipid synthesis and contains pre-Golgi secretory proteins including nascent lipoproteins. J. Biol. Chem. *269*, 27494–27502.

Santel, A., and Fuller, M.T. (2001). Control of mitochondrial morphology by a human mitofusin. J. Cell Sci. *114*, 867–874.

Schreiner, B., Hedskog, L., Wiehager, B., and Ankarcrona, M. (2015). Amyloid-β peptides are generated in mitochondria-associated endoplasmic reticulum membranes. J. Alzheimers Dis. *43*, 369–374.

Shibata, Y., Voss, C., Rist, J.M., Hu, J., Rapoport, T.A., Prinz, W.A., and Voeltz, G.K. (2008). The reticulon and DP1/Yop1p proteins form immobile oligomers in the tubular endoplasmic reticulum. J. Biol. Chem. *283*, 18892–18904.

Stoica, R., De Vos, K.J., Paillusson, S., Mueller, S., Sancho, R.M., Lau, K.F., Vizcay-Barrena, G., Lin, W.L., Xu, Y.F., Lewis, J., et al. (2014). ER-mitochondria associations are regulated by the VAPB-PTPIP51 interaction and are disrupted by ALS/FTD-associated TDP-43. Nat. Commun. *5*, 3996.

Su, B., Wang, X., Zheng, L., Perry, G., Smith, M.A., and Zhu, X. (2010). Abnormal mitochondrial dynamics and neurodegenerative diseases. Biochim. Biophys. Acta *1802*, 135–142.

Sugiura, A., Nagashima, S., Tokuyama, T., Amo, T., Matsuki, Y., Ishido, S., Kudo, Y., McBride, H.M., Fukuda, T., Matsushita, N., et al. (2013). MITOL regulates endoplasmic reticulum-mitochondria contacts via Mitofusin2. Mol. Cell *51*, 20–34.

Swerdlow, R.H., Burns, J.M., and Khan, S.M. (2010). The Alzheimer's disease mitochondrial cascade hypothesis. J. Alzheimers Dis. *20* (*Suppl 2*), S265–S279.

Szabadkai, G., Bianchi, K., Várnai, P., De Stefani, D., Wieckowski, M.R., Cavagna, D., Nagy, A.I., Balla, T., and Rizzuto, R. (2006). Chaperone-mediated coupling of endoplasmic reticulum and mitochondrial Ca^{2+} channels. J. Cell Biol. *175*, 901–911.

Toescu, E.C., and Verkhratsky, A. (2004). Ca^{2+} and mitochondria as substrates for deficits in synaptic plasticity in normal brain ageing. J. Cell. Mol. Med. *8*, 181–190.

Vance, J.E. (1990). Phospholipid synthesis in a membrane fraction associated with mitochondria. J. Biol. Chem. *265*, 7248–7256.

Vance, J.E. (2014). MAM (mitochondria-associated membranes) in mammalian cells: lipids and beyond. Biochim. Biophys. Acta *1841*, 595–609.

Wang, X., Su, B., Lee, H.G., Li, X., Perry, G., Smith, M.A., and Zhu, X. (2009). Impaired balance of mitochondrial fission and fusion in Alzheimer's disease. J. Neurosci. *29*, 9090–9103.

Wang, P.T., Garcin, P.O., Fu, M., Masoudi, M., St-Pierre, P., Panté, N., and Nabi, I.R. (2015). Distinct mechanisms controlling rough and smooth endoplasmic reticulum contacts with mitochondria. J. Cell Sci. *128*, 2759–2765.

Westermann, B. (2010). Mitochondrial fusion and fission in cell life and death. Nat. Rev. Mol. Cell Biol. *11*, 872–884.

Zampese, E., Fasolato, C., Kipanyula, M.J., Bortolozzi, M., Pozzan, T., and Pizzo, P. (2011). Presenilin 2 modulates endoplasmic reticulum (ER)-mitochondria interactions and Ca^{2+} cross-talk. Proc. Natl. Acad. Sci. USA *108*, 2777–2782.

Zatti, G., Ghidoni, R., Barbiero, L., Binetti, G., Pozzan, T., Fasolato, C., and Pizzo, P. (2004). The presenilin 2 M239I mutation associated with familial Alzheimer's disease reduces Ca^{2+} release from intracellular stores. Neurobiol. Dis. *15*, 269–278.

Zatti, G., Burgo, A., Giacomello, M., Barbiero, L., Ghidoni, R., Sinigaglia, G., Florean, C., Bagnoli, S., Binetti, G., Sorbi, S., et al. (2006). Presenilin mutations linked to familial Alzheimer's disease reduce endoplasmic reticulum and Golgi apparatus calcium levels. Cell Calcium *39*, 539–550.